CrossMark

ORIGINAL PAPER

A glassy carbon electrode modified with a nanocomposite consisting of MoS$_2$ and reduced graphene oxide for electrochemical simultaneous determination of ascorbic acid, dopamine, and uric acid

Liwen Xing[1] · Zhanfang Ma[1]

Abstract We describe the synthesis of a hybrid nanocomposite consisting of MoS$_2$ and reduced graphene oxide (MoS$_2$/rGO) by a one-pot hydrothermal process, and the use of the material in an amperometric sensor. Scanning electron microscopy and nitrogen adsorption-desorption tests revealed that the nanocomposite possesses a porous and flower-like structure and a large specific surface. Cyclic voltammetry and differential pulse voltammetry demonstrated the nanocomposite to perform excellently in the electrochemical oxidation of ascorbic acid (AA), dopamine (DA), and uric acid (UA), respectively. The oxidation potentials are well separated (oxidation peaks at −64, 168 and 320 mV vs. Ag/AgCl) for AA, DA, and UA, and the respective detection sensitivities are strongly enhanced (0.12, 4.11 and 1.59 μA μM^{-1} cm^{-2}). The sensor was applied to the detection of the three species in spiked human serum samples where it gave recoveries ranging from 98.9 to 104.1 % (for n=3).

✉ Zhanfang Ma
mazhanfang@cnu.edu.cn

1   Department of Chemistry, Capital Normal University,
    Beijing 100048, China

Introduction

Ascorbic acid (AA), dopamine (DA) and uric acid (UA) are considered as crucial small biomolecules in the physiological processes of human metabolism. AA, i.e. vitamin C, is one of the essential nutrients for most mammal, but also associated with various disorders in human body, such as scurvy, mental illness, hepatic disease, infertility, common cold, cancer and AIDS [1, 2]. As one of the most important catecholamine neurotransmitters, DA plays a vital role in the function of central nervous, renal, hormonal and cardiovascular systems, abnormal levels of which may lead to serious neurological disorders, like Parkinson's disease and schizophrenia [3, 4]. UA is the primary end product of purine metabolism, abnormal levels of which in urine and serum was a symptom of several diseases such as gout, hyperuricemia, pneumonia and Lesch-Nyhan syndrome [5, 6]. On the other hand, AA, DA, and UA usually co-exist in human physiological fluids. The simultaneous determination of these three small biomolecules is a challenging issue for the prediction and prevention of multiple diseases. Electrochemical methods are an effective toolbox for the detection of AA, DA, or UA due to their high sensitivity, simplicity, low costs and fast response for analysis [7–12]. However, these three species usually foul the detection electrodes and can be oxidized at almost the same potential at the traditional electrodes [13, 14]. Therefore, the technique difficulties for electrochemically simultaneous determination lie in how to achieve distinguishable oxidation potentials and sensitive current response at modified electrode.

Graphene oxide (rGO) has been considered as a versatile scaffold for nanomaterials to form hybrid nanocomposite with improved properties [15–23]. Compared with pure graphene

🖄 Springer

(GN), rGO was hydrophilic and easily dispersed into many solvents for various modification, due to its defects and numerous oxygen functions (-OH, C=O, -COOH). Up to now, rGO has been used as an effective support matrix to disperse or stabilize noble metal such as Ag, Au, Pt, Pd, and alloys [7–11]. In addition, those hybrid nanocomposites combining rGO sheets with noble metal nanomaterials have been applied to electrochemically simultaneous detection of AA, DA, and UA. However, those methods to composite rGO sheets with precious metal nanomaterials suffered from some disadvantages such as high cost, multiple-step and time-consuming processes [7–11]. Furthermore, the obtained analytical performance based on those nanocomposites, was highly demanded to be improved. For instance, the detection sensitivity was still not high enough and the separation of the oxidation potential was of necessity to be further extended. Therefore, it is urgently necessary to develop alternatives to noble metals to obtain a low-cost and high-performance rGO-based nanocomposite for electrochemically simultaneous detection of small biomolecules in practical applications.

MoS_2-based materials exhibit superior performance in the energy conversion and storage field including solar cells, electrocatalysis, supercapacitors and lithium ions batteries, due to their unique physical and chemical properties such as graphene-like 2D structure, tunable band gap, edge/defective sites and so on [24, 25]. Although there have been increasing reports on the MoS_2-based materials for bioactive macromolecules detection like DNA, micro-RNA and protein [26–28], it is still desirable to develop new MoS_2-based nanocomposite for the detection of small biomolecules such as AA, DA, and UA. Herein, MoS_2/rGO nanocomposite with porous nanostructure, large specific surface area and good electric conductivity, was prepared simply by a one-pot hydrothermal treatment. The MoS_2/rGO nanocomposite combining rGO and MoS_2 was used as electrode material to successfully construct a selective, stable and reproducible electrochemical biosensor for simultaneous detection of AA, DA, and UA.

Experimental

Reagents and apparatus

Graphene oxide (GO) powders (JCGO-99-1-150n; the contents of O and N tested by X-ray photoelectron spectroscopy (XPS) were 20.31 and 1.71 %, respectively) were purchased from JCNANO (Nanjing, China, www.jcnano.com). All the other chemicals were of analytical grade from commercial sources and used without further purification unless otherwise specified. High-resolution transmission electron microscopy (HRTEM) images were taken from a JEOL Model

JEM-2100F TEM at 200 kV (www.jeol.de/electronoptics-en). Scanning electron microscopy (SEM) images were determined with a Hitachi S-4800 microscope (www.hitachi.com). XPS was conducted using an Escalab 250 X-ray Photoelectron Spectroscope (ThermoFisher, American, www.thermoscientific.com). Fourier transform infrared (FTIR) spectra were recorded on FTIR spectroscope (Tensor 37, Bruker, Germany, www.bruker.com). X-ray diffraction (XRD) analysis was performed on a Rigaku D/max-IIB X-ray diffractometer using Cu Kα radiation (λ=1.5418 Å) (www.rigaku.com). An ultrasonic bath (KQ218, 40 kHz, 100 W, China, www.ks-csyq.com) was used as the ultrasonic source. In all the procedures, the double-distilled water (resistivity =18.2 MΩ cm^{-1}) was obtained from an Olst ultrapure K8 apparatus (Olst, Ltd., www.olst.cn). All the electrochemical measurements were carried out at room temperature on CHI-842C electrochemical workstation (Chen-hua Instruments Inc., Shanghai, China, www.chinstruments.com). A three-electrode system was used in the experiment with a glassy carbon electrode (GCE) (ca. 0.0707 cm^2) as the working electrode, an Ag/AgCl electrode (saturated KCl) as reference electrode and a Pt wire electrode as counter electrode, respectively. Phosphate buffer (PB) comprising NaH_2PO_4, Na_2HPO_4, and KCl was used as the supporting electrolyte throughout the experiment without otherwise specification.

Synthesis of MoS_2/rGO nanocomposite

For a typical synthesis [29, 30], 50 mg of GO powders were dispersed into 100 mL of H_2O and ultrasonicated until the mixture turned yellow-brown and clear, indicating GO aqueous suspensions were obtained. Afterward, 0.6 g of Na_2MoO_4 $2H_2O$ and 0.75 g of NH_2CSNH_2 were dissolved into the above GO suspensions (30 mL) and stirred until the solution became homogeneous. Then the mixture solution was transferred into a 50 mL Teflon-lined autoclave and heated in an oven at 220 °C for 24 h. After cooling to room temperature naturally, the black precipitates obtained were centrifuged and washed with double-distilled water and anhydrous ethanol in sequence for three times and then dried under vacuum at 50 °C overnight. For comparison, pure MoS_2 was prepared with the same procedure in the absence of GO.

Electrode preparation

To prepare the working electrode, the dried and ground MoS_2/rGO nanocomposite was dispersed in a mixed solution (the volume ratio of DMF vs water was 3:1) and ultrasonicated until the mixed solution was homogeneous. The concentration of composite suspension was 10 mg mL^{-1}. Then, 10 μL of suspensions were cast onto a mirror-polished and clean GCE and dried under an infrared lamp. The obtained modified

electrode was denoted as MoS$_2$/rGO/GCE and stored at room temperature when not in use. For comparison, the pure MoS$_2$ modified GCE (MoS$_2$/GCE) was prepared in the same way.

Results and discussion

Characterization of the nanocomposite

As shown in Fig. 1a, the pure MoS$_2$ with sheet-like nanostructure tended to tightly stack together, which implied the aggregated nature of the synthesized pure MoS$_2$. In contrast, the MoS$_2$/rGO nanocomposite (Fig. 1b) displayed a loose porous and flower-like nanostructure consisting of 2D petal-like nanoflakes. A representative lamellar structure of the pure MoS$_2$ and MoS$_2$ component in MoS$_2$/rGO nanocomposite can be seen in the inset of Fig. 1a and b, consistent with the (002) plane of hexagonal atomic lattices in bulk MoS$_2$. The interlayer distance of 0.63 nm for MoS$_2$ component in MoS$_2$/rGO nanocomposite was slightly larger than that of 0.61 nm in the pure MoS$_2$, which corresponded to the previous literatures [31, 32].

Crystalline structures of MoS$_2$ and MoS$_2$/rGO nanocomposite were investigated by XRD. As shown in Fig. 2a, both samples displayed the similar typical hexagonal structure of crystalline MoS$_2$ (JCPDS 37-1492). The primary peak of both appeared around 14.06°, corresponding to the diffraction from (002) plane of MoS$_2$ with the layer-to-layer spacing of 0.62 nm [29, 30]. This was also consistent well with the HRTEM results, indicating successful preparation of the nanocomposite. The nitrogen adsorption-desorption isotherms of MoS$_2$ and the MoS$_2$/rGO nanocomposite exhibited type IV with type H3 hysteresis loop and possessed mesoporous structure (Fig. 2b). The specific surface area of MoS$_2$/rGO nanocomposite was measured to be 96.5 m^2 g^{-1}, which was much larger than that of MoS$_2$ (23.6 m^2 g^{-1}). The MoS$_2$/rGO nanocomposite exhibited an average pore size of 14.13 nm which was slightly smaller than 17.69 nm of MoS$_2$ (BJH analysis, the inset of Fig. 2b). Those results implied that increased specific surface area and unique porous nanostructure of the nanocomposite may provide more active sites for the adsorption of target molecules, which contributed to enhancing electrocatalytic performance of the modified electrode [33].

The compositions of the pure MoS$_2$ and MoS$_2$/rGO nanocomposite and chemical states of C, S, and Mo element were then characterized by XPS. The XPS results showed that both samples consisted of Mo, S, C, and O element, and the atomic ratio of Mo to S for both was approximately 1:2 (Fig. S1). As shown in Fig. 3a, four different peaks of C(O)-O, C=O, C-O-C and sp^2-hydridized C-C proved a considerable degree of oxidation in GO while the C 1 s peak-fitting results of MoS$_2$/rGO nanocomposite (Fig. 3b) just exhibited C-C peak and smaller peaks of C=O and C-O-C compared with that of GO. The disappearance of the C(O)-O peak obviously suggested the effective reduction of GO during the one-pot hydrothermal treatment, which was in accordance with FTIR analysis (Fig. S2). As shown in Fig. S3A, the main doublet located at binding energies of 162.03 and 163.18 eV consisted well with the S 2p$_{3/2}$ and S 2p$_{1/2}$ of MoS$_2$, respectively. The S 2 s and Mo 3 days peaks of pure MoS$_2$ are shown in Fig. S3B, and three resolved peaks can be observed. The two main peaks of Mo 3d$_{5/2}$ (229.13 eV) and Mo 3d$_{3/2}$ (232.33 eV) were characteristic of MoS$_2$ and the peak around 226.15 eV was in accordance with S 2 s of MoS$_2$. As for the MoS$_2$/rGO nanocomposite, the above binding energies were all slightly larger than that of pure MoS$_2$ [30]. This result indicated a possible electron transfer between MoS$_2$ layer and rGO sheets in the nanocomposite, which may effectively increase the conductivity and improve the catalytic activity [31].

Electrochemical behaviors of AA, DA, UA at the modified electrode

As displayed in Fig. S4A-C, the individual electrooxidation of AA, DA, and UA occurred at the bare GCE with a large overpotential at different levels and extremely low current response, indicating a sluggish electron transfer process at the bare GCE due to the electrode fouling resulted from the oxidation product of small biomolecules [13, 14]. Compared with the bare GCE, an obvious electrooxidation peak with

Fig. 1 SEM images and HRTEM images (insets) of the pure MoS$_2$ (**a, c**) and the MoS$_2$/rGO nanocomposite (**b, d**), respectively
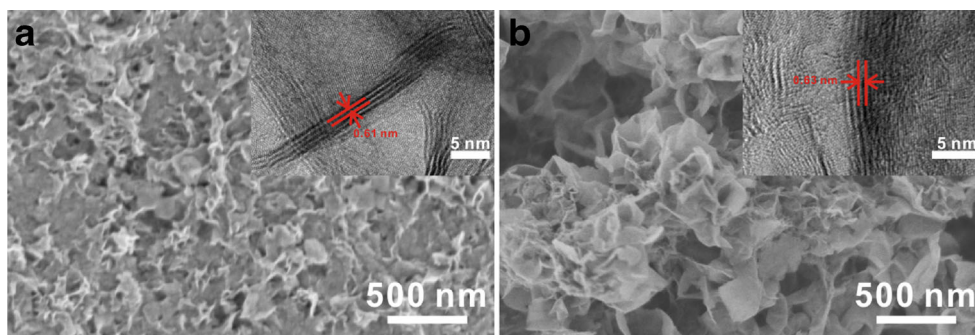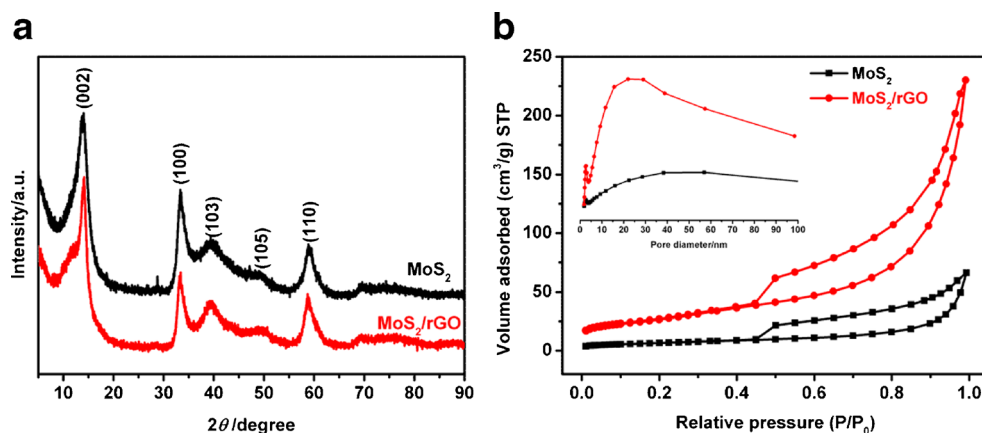
distinct potential shift and high current response appeared at the MoS$_2$/rGO/GCE because of the enhanced conductivity and catalytic activity. As shown in Fig. S4D, a broad, over-lapped and quite small anodic peak appeared at bare GCE while three well-resolved and large oxidation peaks stood out at the MoS$_2$/rGO/GCE. This result obtained demonstrated that the MoS$_2$/rGO/GCE had a rather better capacity to effectively distinguish the oxidation potentials of the three biomolecules than the bare GCE. From Fig. S4A to 4D, the MoS$_2$/GCE only presented a large background current response and no remarkable separating ability. To further verify the separating ability and current sensitivity of the MoS$_2$/rGO/GCE, differential pulse voltammetry (DPV) curves for the oxidation of AA, DA, and UA in their mixture at MoS$_2$/rGO/GCE were shown in Fig. S5. It can be seen that the DPV peaks of these three species were well-resolved with the electrooxidation potentials at about −64 mV (AA), 168 mV (DA), and 320 mV (UA), respectively. Thus, the separation of peak potentials at MoS$_2$/rGO/GCE was 232 and 152 mV for AA-DA and DA-UA, respectively, which was large enough to determine AA, DA, and UA simultaneously. Effects of solution pH and scan rate on the peak potential and current of electrochemical oxidation of the three species were also investigated by DPV (Fig. S6 and S7).

Simultaneous determination of AA, DA, and UA

As shown in Figs. 4, 5 and 6, the DPV responses of MoS$_2$/rGO/GCE toward AA, DA, or UA were displayed when the concentration of one species changed with the other two keeping constant. The peak current of AA was linear to the AA concentrations in the range from 12 to 5402 μM with a regression equation of $I_{p,AA}$ (μA)$=0.0108C_{AA}$ (μM)$+0.738$ ($R^2=0.9994$). The detection sensitivity was calculated to be 0.12 μA μM^{-1} cm^{-2} based on the slope of the regression equation divided by electroactive surface area (ECSA) of the MoS$_2$/rGO/GCE (Fig. S8). The corresponding limit of detection (LOD) was 0.72 μM (S/N=3). As for DA and UA, the peak currents were proportional in the concentration range from 5 to 545 and from 25 to 2745 μM, respectively. The linear functions were $I_{p,DA}$ (μA)$=0.364C_{DA}$ (μM)$+2.758$ ($R^2=0.9988$) and $I_{p,UA}$ (μA)$=0.141C_{UA}$ (μM)$+0.339$ ($R^2=0.9986$), respectively. The corresponding detection sensitivity of DA and UA was 4.11 and 1.59 μA μM^{-1} cm^{-2} while the LOD of DA and UA were 0.05 and 0.46 μM, respectively. The various analytical performances of the electrochemical sensor were compared with those reported in the literature (Table S1). Notably, compared with those high-cost noble metal-based biosensors, MoS$_2$/rGO/GCE exhibited a higher sensitivity,
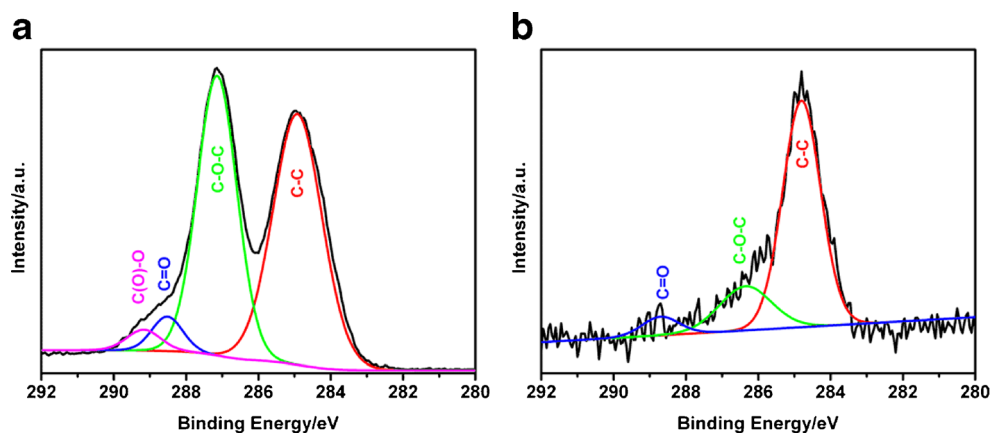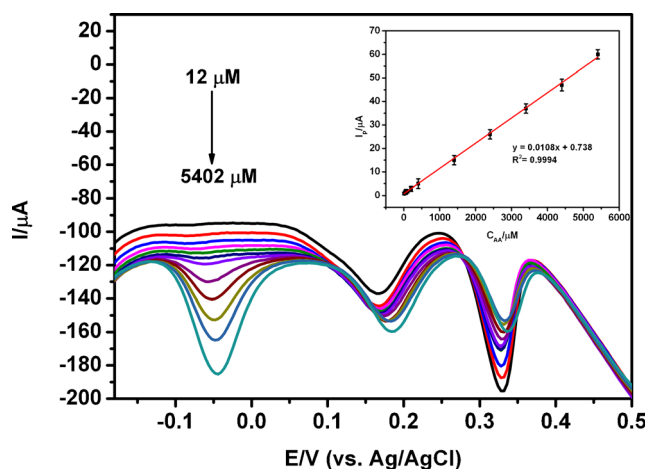
Fig. 4 DPVs of MoS$_2$/rGO/GCE in 0.1 M PB (pH 7.0) containing 100 µM DA, 200 µM UA and different concentration of AA (from inner to outer): 12, 22, 42, 62, 102, 202, 402, 1402, 2402, 3402, 4402, 5402 µM. Insets: plots of peak current I_p vs concentration of AA (data recorded from −0.2 to 0.6 V, vs. Ag/AgCl)

Fig. 6 DPVs of MoS$_2$/rGO/GCE in 0.1 M PB (pH 7.0) containing 1 mM AA, 100 µM DA and different concentration of UA (from inner to outer) 25, 45, 65, 105, 145, 245, 345, 545, 745, 1745, 2745 µM. Insets: plots of peak current I_p vs concentration of UA (data recorded from −0.2 to 0.6 V, vs. Ag/AgCl)

lower detection limit and wider linear range. The MoS$_2$/rGO nanocomposite was thus one of the promising candidates for selective and sensitive determination of AA, DA, and/or UA.

Selectivity, stability and reproducibility

To investigate the anti-interference ability of MoS$_2$/rGO/GCE, the peak current ratio was compared as shown in Fig. S9. I_0, I_1, I_2 meant the DPV current response for 1 mM AA, 100 µM DA, 200 µM UA and I for 1 mM of various interferential compounds and ions. Peak current ratio changed less than ±6 % (Fig. S9), indicating the biosensor exhibited good selectivity for the detection of AA, DA and/or UA. The stability
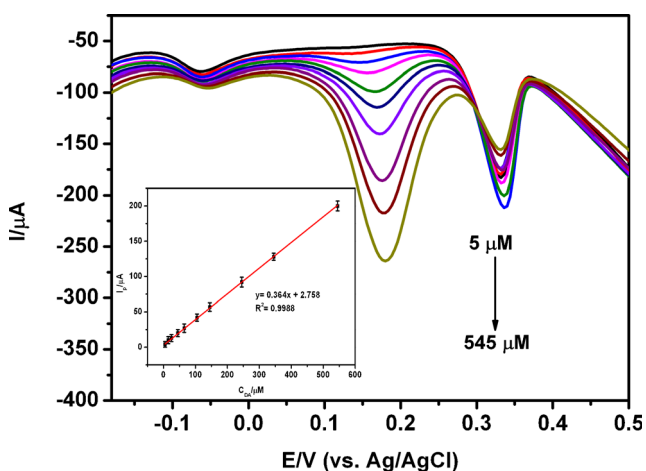
was quite essential for nanocomposite modified electrode to construct the biosensor [34]. The stability of MoS$_2$/rGO/GCE was investigated by CV with 50 circles of continuous scan in 5 mM [Fe(CN)$_6$]$^{3-/4-}$ aqueous solution containing 0.1 M KCl. The results showed that there was a negligible decrease of the voltammetric current during the whole procedures, suggesting that an excellent stability of the electrode (Fig. S10). The reproducibility was studied by five modified electrode prepared independently using the same batch of composite material. By comparing the peak currents in 0.1 M PB (pH 7.0) containing 1 mM AA, 100 µM DA and 200 µM UA, the relative standard deviation (R.S.D) for AA, DA, and UA were 3.52, 2.78, 3.23 %, respectively, indicating excellent reproducibility.

Real sample analysis

To verify the feasibility of the MoS$_2$/rGO/GCE in practical analysis, it was applied to simultaneously detect the concentration of AA, DA, and UA in human serum samples using standard addition method. All the samples was filtrated and diluted with PB (pH 7.0) before the measurements. The analysis data were summarized in Table S2, showing the potential practical application of our biosensor for real samples.

Conclusions

In summary, a facile strategy for preparing MoS$_2$/rGO hybrid nanocomposite has been developed by a one-pot hydrothermal synthesis. Electrochemical measurements demonstrated that the nanocomposite can improve electrocatalytic performance toward oxidation of AA, DA, and UA by enlarging

Fig. 5 DPVs of MoS$_2$/rGO/GCE in 0.1 M PB (pH 7.0) containing 1 mM AA, 200 µM UA and different concentration of DA (from inner to outer): 5, 15, 25, 45, 65, 105, 145, 245, 345, 545 µM. Insets: plots of peak current I_p vs concentration of DA (data recorded from −0.2 to 0.6 V, vs. Ag/AgCl)
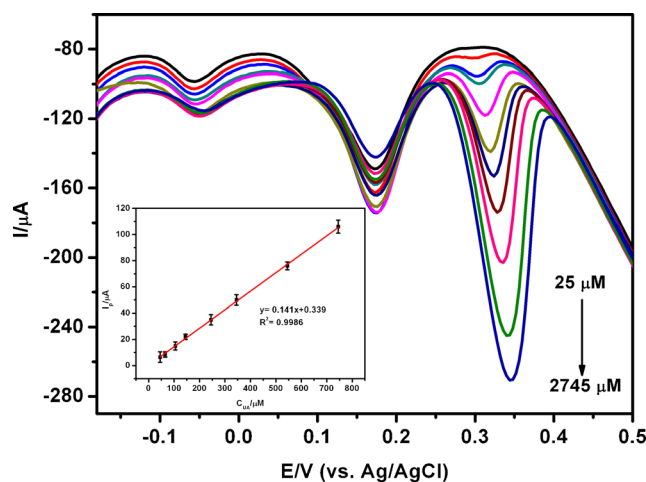
peak separation and increasing peak current due to its unique porous nanostructure, large specific surface area and good electric conductivity. Simultaneous detection of AA, DA, and UA was achieved in a wide concentration range with high sensitivity and good selectivity. The biosensor herein may be applied to selectively detect other bioactive biomolecules such as epinephrine, nor-epinephrine, etc. Furthermore, other disulphide-based nano-composites with rGO may also possess a wide range of applications in biosensors.

References

1. Zheng YJ, Huang ZJ, Zhao CF, Weng SH, Zheng W, Lin XH (2013) A gold electrode with a flower-like gold nanostructure for simultaneous determination of dopamine and ascorbic acid. Microchim Acta 180:537–544
2. Zhao DY, Fan DW, Wang JP, Xu CX (2015) Hierarchical nanoporous platinum-copper alloy for simultaneous electrochemical determination of ascorbic acid, dopamine, and uric acid. Microchim Acta 182:1345–1352
3. Wang Y, Li YM, Tang LH, Lu J, Li JH (2009) Application of graphene-modified electrode for selective detection of dopamine. Electrochem Commun 11:889–892
4. Wang HW, Ren FF, Yue RR, Wang CQ, Zhai CY, Du YK (2014) Macroporous flower-like graphene-nanosheet clusters used for electrochemical determination of dopamine. Colloids Surf A 448:181–185
5. Du J, Yue RR, Yao ZQ, Jiang FX, Du YK, Yang P, Wang CY (2013) Nonenzymatic uric acid electrochemical sensor based on graphene-modified carbon fiber electrode. Colloids Surf A 419:94–99
6. Wang Y, Xiao Y (2012) Glassy carbon electrode modified with poly(dibromofluorescein) for the selective determination of dopamine and uric acid in the presence of ascorbic acid. Microchim Acta 178:123–130
7. Yan J, Liu S, Zhang ZQ, He GW, Zhou P, Liang HY, Tian LL, Zhou XM, Jiang HJ (2013) Simultaneous electrochemical detection of ascorbic acid, dopamine and uric acid based on graphene anchored with Pd-Pt nanoparticles. Colloids Surf B 11:392–397
8. Wu GH, Wu YF, Liu XW, Rong MC, Chen XM, Chen X (2012) An electrochemical ascorbic acid sensor based on palladium nanoparticles supported on graphene oxide. Anal Chim Acta 745:33–37
9. Zhou CL, Li S, Zhu W, Pang HJ, Ma HY (2013) A sensor of a polyoxometalate and Au-Pd alloy for simultaneously detection of dopamine and ascorbic acid. Electrochim Acta 113:454–463
10. Wang X, Wu M, Tang WR, Zhu Y, Wang LW, Wang QJ, He PG, Fang YZ (2013) Simultaneous electrochemical determination of ascorbic acid, dopamine and uric acid using a palladium nanoparticle/graphene/chitosan modified electrode. J Electroanal Chem 695:10–16
11. Wang CQ, Du J, Wang HW, Zou CE, Jiang FX, Yang P, Du YK (2014) A facile electrochemical sensor based on reduced graphene oxide and Au nanoplates modified glassy carbon electrode for simultaneous detection of ascorbic acid, dopamine and uric acid. Sens Actuators B 204:302–309
12. Huang YP, Miao YE, Ji SS, Tjiu WW, Liu TX (2014) Electrospun carbon nanofibers decorated with Ag-Pt bimetallic nanoparticles for selective detection of dopamine. ACS Appl Mater Interface 6:12449–12456
13. Huang JS, Liu Y, Hou HQ, You TY (2008) Simultaneous electrochemical determination of dopamine, uric acid and ascorbic acid using palladium nanoparticle-loaded carbon nanofibers modified electrode. Biosens Bioelectron 24:632–637
14. Sheng ZH, Zheng XQ, Xu JY, Bao WJ, Wang FB, Xia XH (2012) Electrochemical sensor based on nitrogen doped graphene: simultaneous determination of ascorbic acid, dopamine and uric acid. Biosens Bioelectron 34:125–131
15. Chen D, Tang LH, Li JH (2010) Graphene-based materials in electrochemistry. Chem Soc Rev 39:3157–3180
16. Chen D, Feng HB, Li JH (2012) Graphene oxide: preparation, functionalization, and electrochemical applications. Chem Rev 112:6027–6053
17. Liu N, Liu ZM, Han HL, Ma ZF (2014) Graphene oxide reduced directly by redox probes for multiplexed detection of tumor markers. J Mater Chem B 2:3292–3298
18. Hao MJ, Liu N, Ma ZF (2013) A new luminol chemiluminescence sensor for glucose based on pH-dependent graphene oxide. Analyst 138:4393–4397
19. Wang LY, Liu N, Ma ZF (2015) Novel gold-decorated polyaniline derivatives as redox-active species for simultaneous detection of three biomarkers of lung cancer. J Mater Chem B 3:2867–2872
20. Guo SJ, Dong SJ (2011) Graphene nanosheet: synthesis, molecular engineering, thin film, hybrids, and energy and analytical applications. Chem Soc Rev 40:2644–2672
21. Wang Y, Shao YY, Matson DW, Li JH, Lin YH (2010) Nitrogen-doped graphene and its application in electrochemical biosensing. ACS Nano 4:1790–1798
22. Lei W, Si WM, Xu YJ, Gu ZY, Hao QL (2014) Conducting polymer composites with graphene for use in chemical sensors and biosensors. Microchim Acta 181:707–722
23. Sanghavi BJ, Wolfbeis OS, Hirsch T, Swami NS (2015) Nanomaterial-based electrochemical sensing of neurological drugs and neurotransmitters. Microchim Acta 182:1–41
24. Wang H, Feng HB, Li JH (2014) Graphene and graphene-like layered transition metal dichalcogenides in energy conversion and storage. Small 10:2165–2181
25. Huang X, Zeng ZY, Zhang H (2013) Metal dichalcogenide nanosheets: preparation, properties and applications. Chem Soc Rev 42:1934–1946
26. Su S, Chao J, Pan D, Wang LH, Fan CH (2015) Electrochemical sensors using two-dimensional layered nanomaterials. Electroanalysis 27:1062–1072
27. Ge J, Ou EC, Yu RQ, Chu X (2014) A novel aptameric nanobiosensor based on self-assembled DNA-MoS$_2$ nanosheet architecture for biomolecule detection. J Mater Chem B 2:625–628
28. Huang JH, Ye L, Gao X, Li H, Xu JB, Li ZG (2015) Molybdenum disulfide-based amplified fluorescence DNA detection using hybridization chain reactions. J Mater Chem B 3:2395–2401
29. Min SX, Lu GX (2012) Sites for high efficient photocatalytic hydrogen evolution on a limited-layered MoS$_2$ cocatalyst confined on graphene sheets—the role of graphene. J Phys Chem C 116:25415–25424
30. Li HL, Yu K, Fu H, Guo BJ, Lei X, Zhu ZQ (2015) MoS$_2$/graphene hybrid nanoflowers with enhanced electrochemical performances as Anode for lithium-ion batteries. J Phys Chem C 119:7959–7968

31. Li YG, Wang HL, Xie LM, Liang YY, Hong GS, Dai HJ (2011) MoS$_2$ nanoparticles grown on graphene: an advanced catalyst for the hydrogen evolution reaction. J Am Chem Soc 133:7296–7299

32. Xie JF, Zhang H, Li S, Wang RX, Sun X, Zhou M, Zhou JF, Lou XW, Xie Y (2013) Defect-rich MoS$_2$ ultrathin nanosheets with additional active edge sites for enhanced electrocatalytic hydrogen evolution. Adv Mater 25:5807–5813

33. Punckt C, Pope MA, Aksay IA (2014) High selectivity of porous graphene electrodes solely due to transport and pore depletion effects. J Phys Chem C 118:22635–22642

34. Xu T, Liu N, Yuan J, Ma ZF (2015) Triple tumor markers assay based on carbon-gold nanocomposite. Biosens Bioelectron 70:161–166